Interband and Intraband Optical Studies of PbSe Colloidal Quantum Dots

Brian L. Wehrenberg, Congjun Wang, and Philippe Guyot-Sionnest*

James Franck Institute, The University of Chicago, 5640 South Ellis Avenue, Chicago, Illinois 60637

Received: May 10, 2002; In Final Form: July 25, 2002

PbSe nanocrystal colloids exhibit a well-defined excitonic structure with the lowest energy exciton tuning from 0.5 to 1 eV, as a function of size. Band-edge fluorescence is observed from 1.2 to 2 μm with a small Stokes shift, sub-μs lifetime, and near-unity quantum yield. Upon pumping at 1.064 μm, the first exciton decay is consistent with radiative relaxation at low pump intensity and with Auger recombination at higher pump intensities. Optically induced absorption is observed at approximately midgap. These transitions exhibit strengths similar to the interband exciton and are size-tunable. They are assigned to the $1S_{e,h}-1P_{e,h}$ and $1P_{e,h}-1D_{e,h}$ intraband excitations. Intraband pump−probe measurements of the $1S_{e,h}-1P_{e,h}$ transition reveal a short lifetime and the absence of the phonon bottleneck.

I. Introduction

For over 2 decades, semiconductor colloidal quantum dots have been studied both experimentally[1] and theoretically.[2] The attention is owed not only to academic interest in a system which wonderfully demonstrates quantum mechanical effects and lies in a realm between bulk and atomic properties, but also because of its possible applications. Of particular interest are the optical properties of quantum dots. Owing to the small size of the dots, discrete optical transitions can be tuned with size. This fact, coupled with the flexibility of chemical synthesis of quantum dots, makes them chemicals in a bottle with strong size-tunable transitions.

PbSe, with a band gap in the mid-infared and a small effective mass, is an interesting material for infared application. In the visible, organic dyes are usually superior to quantum dots in terms of their fluorescence efficiency, but infared organic dyes are very poor fluorophores. The only efficient infrared fluorophores are the rare-earth ions with small cross sections and microsecond lifetimes. Soluble infrared fluorophores, which are both efficient and possess shorter lifetimes, may find unique applications for fluorescent imaging and tagging in the near-IR spectral range where biological tissues are relatively transparent, or as fluorescent materials in the fiber communication range of 1.3−1.5 microns. It is also noteworthy that PbSe has a very large optical index of refraction of ∼4.6 and may be a potential material for photonic band gap applications. Tuning the optical band edge while keeping a high optical constant is an interesting possibility with PbSe quantum dots.

Over the past few years, highly monodisperse PbS and PbSe nanocrystals have been obtained in an oxide glass host.[3−7] These materials show a well-defined excitonic structure[8] which can be readily size tuned from 0.5 to 1.0 eV. The **k·p** approximation has been applied to these materials,[9] and it has been shown that the simplistic parabolic band model is not such a poor approximation for PbSe quantum dots, unlike for II−VI and III−V materials[2] which possess more complex band structures. Although a glass host has its advantage, liquid solutions of colloids are necessary for applications requiring further processing of the nanocrystals. For many years, the preparation of a monodisperse solution of IV−VI colloids was limited to one specific size of PbS nanocrystals.[10] Recently, Murray and coworkers reported the first synthesis of highly monodisperse and size-tunable PbSe colloidal nanocrystals.[11] Here, we report on the interband absorption and fluorescence as well as the intraband absorption of PbSe colloidal quantum dots.

II. Experimental Section

All dots used in this study were oleic acid capped PbSe quantum dots prepared at moderate temperatures in organic solvents. The basic synthetic scheme briefly described by Murray et al.[11] was elaborated upon to provide monodisperse samples. Lead(II) acetate trihydrate (0.65 g) is dissolved in a solution of phenyl ether (2 mL), oleic acid (1.5 mL), and trioctylphosphine (8 mL) (flask 1). This flask, along with a separate flask (flask 2) of phenyl ether (10 mL), is heated under vacuum for an hour at 85 °C. Flask 1 is then cooled to 45 °C under an inert atmosphere of argon, while flask 2, also under argon, is heated to between 180 and 210 °C. Trioctylphosphine selenium (1.7 mL 1M TOPSe) is then added to flask 1. The contents of flask 1 are then rapidly injected into flask 2. After injection, flask 2 cools to between 110 and 130 °C, at which temperature the dots are allowed to grow for 1−10 min. The injection and growth temperatures are varied within the ranges given above to control the spectral position of the first exciton peak. For example, an injection temperature of 180 °C coupled with a growth temperature of 110 °C and a short growth time (∼1 min) will yield a sample with an exciton around 1.03 eV, whereas injection and growth temperatures of 210 and 130 °C, respectively, and a longer growth time (3 min) yield dots with a 0.53 eV exciton. After being cooled to room temperature the dots are precipitated out of solution with methanol, separated by centrifuge and stored dry. The synthetic procedure is simple and reproducible. Furthermore, since the preparation of the quantum dots involves relatively unreactive chemicals, it can be carried out in a hood, without the need for a glovebox.

The materials were characterized by transmission electron microscopy (TEM), X-ray diffraction, and by linear-IR absorption spectroscopy. Linear absorption spectra were taken with a Fourier transform infrared spectrometer operating from 11000 to 2000 cm^{-1}. Figure 1 demonstrates the size tunability of the interband absorption features and the rather tight size selection. The interband features are sharp enough to show not only the

10.1021/jp021187e CCC: $22.00
Published on Web 09/24/2002

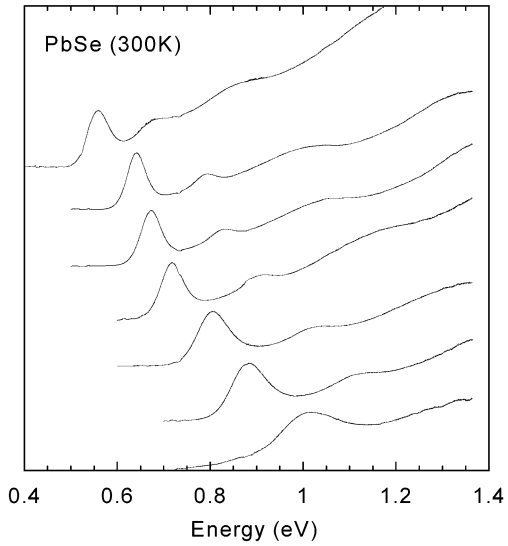

Figure 1. Absorption spectra of PbSe quantum dot samples of different sizes. Samples are at room temperature in chloroform solvent.

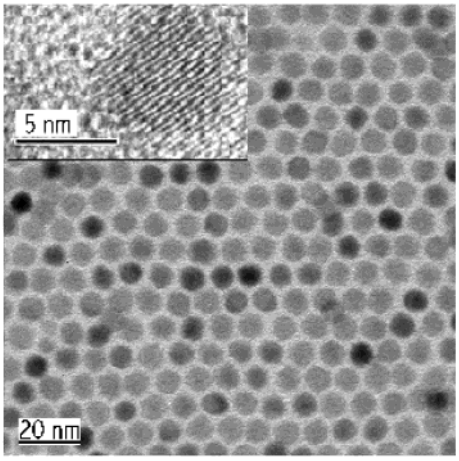

Figure 2. TEM micrograph of a PbSe colloidal quantum dot sample with a room-temperature exciton at 0.587 eV. Inset shows the lattice fringes of one dot from a sample with a 0.688 eV room-temperature exciton.

first, but the second and often the third exciton features. The first exciton is quite narrow, with $\sigma_E/(E - E_g) \sim 4\%$ for the best samples, indicative of a tight size distribution. From TEM studies, average diameters of 8.1, 7.1, and 5.8 nm were determined for samples with 0.587, 0.688, and 0.865 eV first exciton peaks, respectively. Figure 2 shows a TEM micrograph of a sample with a 0.587 eV first exciton peak. This picture represents the size-distribution from the reaction without size-selective precipitation steps. From Figure 2 the distribution of sizes for this sample of dots was determined to have a standard deviation of only ~5%. Regular lattice fringes are seen throughout the nanocrystals in high-resolution TEM micrographs and powder X-ray diffraction confirms the bulk cubic crystal structure.

The fluorescence is detected with a cooled HgCdTe photovoltaic detector or an InGaAs photodiode for increased sensitivity below 1.7 μm. The colloids are dissolved in chloroform or toluene and fill a 2 mm glass cell. The cell is excited in front-face geometry by a laser pulse at 1.064 μm. The fluorescence is collected by a paraboloid mirror and sent through a monochromator. The monochromator is a home-built 0.11 m Czerny−Turner design. The mirrors are off-axis paraboloids with focal lengths of 11 cm and diameters of 5 cm. The grating is flat

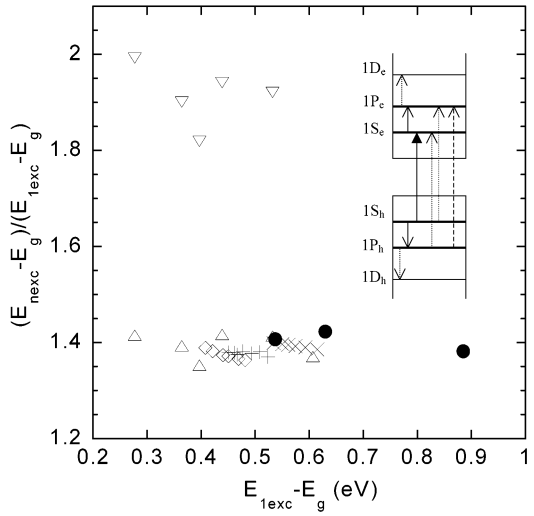

Figure 3. Second and third exciton confinement energies divided by the first confinement energy as a function of the first exciton confinement energy for several samples. Room-temperature data (△ and ▽) data taken at several temperatures between 80 and 300 K for three samples (◇, +, and ×). Also plotted are the $1S_{e,h}-1P_{e,h}$ intraband transition energies (●) at 7 K for three samples as described in the text.

5×5 cm^2 aluminum coated with 600 grooves per mm. With a 1 mm entrance slit imaged on the 1 mm^2 detector area, the wavelength resolution is ~20 nm from 1 to 2 μm. The wavelength scanning is calibrated by recording the multiple orders of scattered 1.064 μm radiation.

For low-temperature linear-IR spectroscopy and the laser studies the samples are dissolved in 2,2,4,4,6,8,8-heptamethylnonane (a low-temperature glass former) and fill a cell with two ZnS windows separated by a 0.75 mm Teflon spacer. The cell is loaded into a He flow cryostat and cooled to as low as 7K.

The laser system is based on an active-passive mode locked Nd:Yag laser operating at 25 Hz. The laser cavity produces both a single pulse of 8 ps duration and a train of pulses at 1.064 μm. A portion of the single pulse is used to excite the interband transition in the sample. The train of pulses is first frequency doubled and then used to pump a grating-tuned optical parametric oscillator (OPO). The OPO produces tunable near-IR light in the 1.2−1.8 μm range. For interband studies the OPO output is amplified to the desired power (~10 μJ/pulse) by mixing with the single pulse in a $AgGaS_2$ crystal. For the intraband studies, we use the difference-frequency output from the $AgGaS_2$ crystal. This difference frequency pulse is then used as the pump and probe beam in the intraband studies. Delay lines in both the 1.064 μm interband pump line and the tunable intraband pump line allow us to vary the delay between the three pulses arriving at the sample.

III. Results and Discussion

A. Linear Absorption Spectroscopy. Figure 1 shows the linear absorption for different samples of PbSe quantum dots. The spectra were accurately fit with a sum of two to four Gaussian curves corresponding to each visible structure and a broad background (either a broad Gaussian at high energy or a power law starting at the band edge). The confinement energies are then extracted by subtracting the band gap energy taken at the appropriate temperature, $E_g(\text{meV}) = 125 + (400 + 0.256T^2)^{1/2}$.[12] Figure 3 shows the confinement energy of the second and third excitons as a function of the confinement

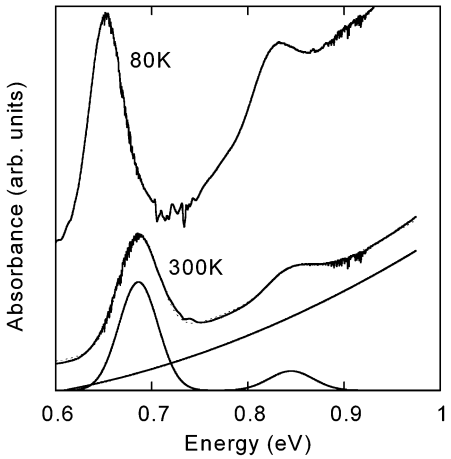

Figure 4. Absorption spectra at 80 and 300 K for a PbSe sample in HMN (—). Also shown are the fitting elements for the 300 K spectra and the resulting fit (dotted line).

energy of the first exciton. Taking the first exciton confinement energy as a reference, the second exciton confinement energy is consistently ~1.4 and the third exciton confinement energy is ~1.9.

The band gap of PbSe tunes strongly with temperature. This leads to a shift of the exciton features,[5] as shown in Figure 4. The temperature dependence of the first and second exciton was recorded for several samples between 298 and 80 K, and the results are plotted in Figure 3 as well. Although temperature strongly affects the confinement energy of the first exciton, the relative ratios remain approximately constant.

The parabolic model (constant effective mass) applied to an infinite spherical potential leads to confinement energy levels given by $\alpha_{n,l}h^2/8m_{\text{eff}}R^2$, where for the first three levels $\alpha_{n,l} = 1$ (1S), 2.04 (1P), 3.36 (1D). The confinement energy of the 1P state is thus about twice that of the 1S state. The third exciton, which has approximately twice the confinement energy of the first exciton, is therefore assigned to the $1P_h-1P_e$ transition. The second exciton is assigned to both the $1P_h-1S_e$ and $1S_h-1P_e$ transitions. This assignment is supported by the intraband measurement reported later.

Although reasonable according to the energy considerations, the assignment of the second exciton is troublesome, since an S to P interband transition is forbidden by parity. Yet the second exciton is not weak, carrying about one-fourth of the weight of the first exciton. It could be that the parabolic model is inadequate, yet the inclusion of nonparabolicity mostly changes the energy vs size relationship but does not remove the parity selection rule.[9] Andreev and Lipowskii reported that inclusion of band anisotropy could make the second transition allowed by a mixing of the states.[13] Alternative possibilities for breaking the parity selection rule are polar shape asymmetry, permanent dipole moment,[14] or quadrupolar transitions.

B. Fluorescence. The PbSe nanocrystal colloids fluoresce efficiently. Figure 5 shows the fluorescence of samples of different sizes. Size control provides a simple method of tuning the fluorescence in the 1.3 and 1.5 μm range, and extending beyond 2 μm.

The small Stokes shift of 22 meV seen in Figure 6 is consistent with band-edge emission. The Stokes shift is only about 4% of the confinement energy. Monodisperse CdSe nanocrystal solutions exhibit a larger nonresonant Stokes shift of about 10% to 15% of the confinement energy.[15] The small Stokes shift of PbSe nanocrystals is not only a reflection of the narrow size dispersion of the sample, but may be also indicative

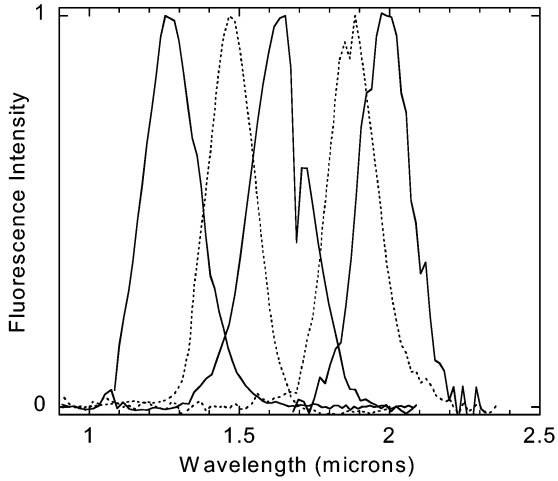

Figure 5. Room-temperature fluorescence of five PbSe nanocrystal samples of different sizes excited by a 1.064 μm laser pulse. Chloroform has sharp absorption features around 1.7 and 1.85 μm.

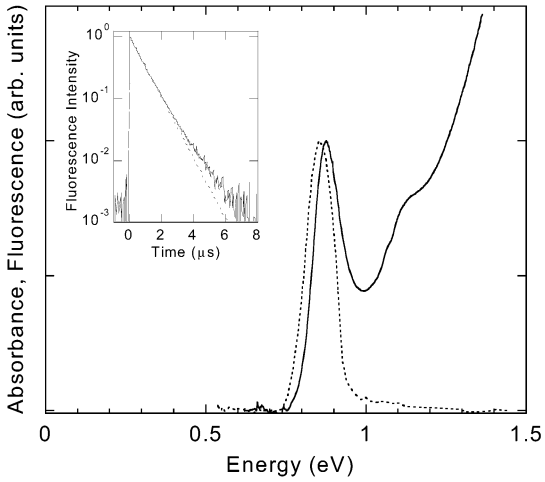

Figure 6. Fluorescence (- -) and absorption (—) spectra of a PbSe quantum dot sample. The inset shows the fluorescence decay on a μs time scale.

of the simpler exciton structure as compared with CdSe. PbSe does not have the hexagonal crystal field splitting and the exchange interaction should be smaller, since for similar confinement energies the PbSe nanocrystals are larger. The simpler band-edge structure is likely to help the fluorescence efficiency.

For the determination of the quantum yield, we used the infrared dye IR#26 (Lamda-Physik, Lambdachrome no. 1080, CAS 76871-75-5). To our knowledge this is the most efficient infrared dye commercially available and it is very photostable. The quantum yield of IR no. 26, determined from both lifetime measurements and absolute determination is reported to be 5×10^{-3}.[16,17] Measurements were also taken on the less efficient dyes IR no. 1 and IR no. 5 and their respective efficiencies were found to be in the reported ratios to IR no. 26. Adjusting the concentrations to obtain similar optical densities of ~0.3, the PbSe sample shown in Figure 6 is about 180 times more efficient than IR no. 26! This gives a quantum efficiency of 85%. The high fluorescence efficiency indicates that trapping processes are ineffective and that the surface is well-passivated by oleic acid. Cooling a sample to 80 K did not lead to a noticeable increase in the fluorescence intensity, although a red shift and a narrowing of the fluorescence was observed as expected. Since IR no. 26 fluoresces in the 1.1−1.3 μm range

and the PbSe sample fluoresces in the 1.3−1.5 μm range, there are issues of proper normalization. The data were corrected for the resolution of the monochromator and the efficiency of the detector, but were not corrected for the unknown efficiency of the grating. The determination of the quantum yield should ultimately be confirmed by calibrated sources. Nevertheless, the PbSe nanocrystals are very efficient infared fluorophores and appear to be more efficient than the other infrared emitting colloidal quantum dots, such as core−shell InAs[18] and Hg−Te based materials.[19]

The fluorescence lifetime was determined with the HgCdTe detector that has a pulse response of 30 ns. The inset in Figure 6 shows the decay for a sample with an exciton at 0.8 eV. The fluorescence decay is rather slow and nearly single exponential with a time constant of 0.88 μs. The lifetime is similar to low-temperature fluorescence lifetimes of CdSe quantum dots where a triplet transition is involved.[2] Yet the similarity is misleading and it is instructive to estimate and compare the singlet radiative lifetimes of PbSe and CdSe quantum dots.

In quantum dots, the momentum transition moment of the first exciton is $\langle 1S_h|p|1S_e\rangle = P$, where P is the Kane interband parameter given by $2P^2/m_0$, and m_0 is the free mass of the electron. For PbSe and CdSe, $2P^2/m_0$ is ~3 eV[1] and 17.5 eV,[20] respectively. The oscillator strength of the first exciton is then $f = 2P^2/m_0E_{1S_h1S_e}$. For comparison, if we take the same 0.4 eV confinement energy in addition to the bulk band-gaps, then $f \sim 4$ and $f \sim 9$ for the first exciton of PbSe and CdSe, respectively. The radiative lifetime of a dipole in a host of optical dielectric constant ϵ_1 is given by $T_1^{-1} = 2e^2\omega\epsilon_1^{1/2}f/3m_0c^3$.[21] Taking $\epsilon_1 \sim 2.1$ for chloroform, one arrives at $T_1 \sim 25$ ns and $T_1 \sim 1$ ns for PbSe and CdSe, respectively. However, the above expression for the radiative lifetime does not take into account the screening of the radiating field inside the quantum dot. If the nanocrystal is spherical, the internal field is weaker by a factor $3\epsilon_1/(\epsilon_2 + 2\epsilon_1)$, and thus the radiative lifetime is longer by the factor $[3\epsilon_1/(\epsilon_2 + 2\epsilon_1)]^{-2}$, where ϵ_2 is the semiconductor optical dielectric constant. The semiconductor optical dielectric constants are ~23[12] for PbSe and ~6[22] for CdSe. The estimated radiative lifetimes then become $T_1 \sim 0.4$ μs and ~3 ns for PbSe and CdSe, respectively. These estimates show that there is no need to invoke a triplet or quasi-forbidden transition to explain the long radiative lifetimes in PbSe and that sub-microsecond radiative lifetimes should be expected in IV−VI colloidal quantum dots with high optical dielectric constants.

C. Time-Resolved Interband Spectroscopy. The dynamics of the interband transition were studied in order to gain further insights into the relaxation mechanism of the photoexcited nanocrystals. Data for the optical bleach of the absorption are shown for a sample with a room temperature first exciton at 0.817 eV. The bleach dynamics of this sample at 80 K are shown in Figure 7 for different incident energies of the 1.064 μm pump beam. The bleach data are normalized to the optical density of the sample and at high pump power the bleach nears unity. We note that the 1.064 μm pump beam excites the second excitons, $1S_h-1P_e$, $1P_e-1S_h$. The bleach of the first exciton appears instantaneously, indicating that depopulation of the $1P_{e,h}$ to $1S_{e,h}$ states takes place within the 11 ps pulses used in this study. An attempt to directly measure the 1P-1S lifetimes is described in the last section.

At low pump power, the first exciton bleach shows a fast (~200 ps) and slow decay component (fit as a constant offset in Figure 7). The faster component may be due to internal cooling or some fraction of nonradiative recombination while the slow component (the constant offset on this ns time scale) is at least consistent with the observed slow radiative relaxation.

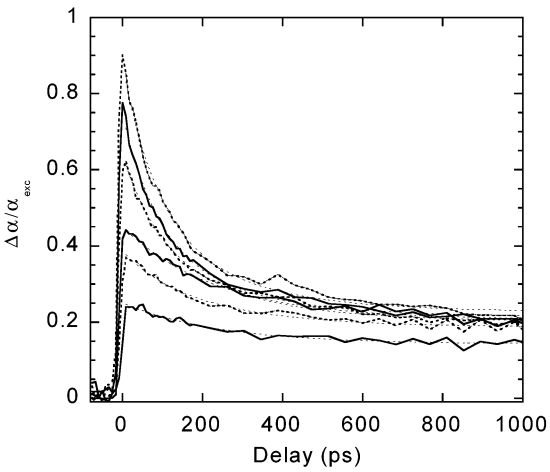

Figure 7. Time-resolved bleach of the first exciton at 0.817 eV of a PbSe quantum dot sample in HMN at 77 K shown for increasing 1.064 μm pump powers from 6.5 to 35 mW (— and - -). The decays were fit as the sum of two exponentials (85 and 240 ps) and an offset corresponding to very long lifetime (—). The 85 ps exponential is required to fit the data with an initial bleach larger than ~0.5. The initial value of the 240 ps exponential term is about 50% of the offset magnitude in the fits.

As the pump power is increased, another decay mechanism with a short lifetime is introduced. This component has a lifetime of 85 ± 10 ps. The bulk Auger parameter for PbSe is $\gamma = 1.1 \pm 0.3 \times 10^{-28}$ cm^6/s.[23] The two-exciton Auger lifetime can then be estimated as $T_{auger}^{-1} = \gamma(2/V)^2$, where V is the nanocrystal volume. For a 6.5 nm diameter quantum dot, this yields a lifetime of 47 ± 13 ps, which is in fair agreement with the 85 ps lifetime observed experimentally. Thus, we assign the fast, power-dependent component to a two-exciton Auger recombination.

D. Intraband Spectroscopy. Materials with optical transitions in the 3−5 μm and 8−12 μm regions, where the atmosphere is transparent, would be of interest for earth based and satellite communications. It is difficult to make high quality materials with mid-infared interband transitions. Interssuband quantum wells and intraband quantum dots are a successful alternative to more conventional materials.[24] It is with the above consideration that our group previously engaged in intraband spectroscopic studies of CdSe, CdS, InP, and ZnO colloidal quantum dots.[25] Upon photoexcitation or direct electron injection, these materials exhibit the intraband $1S_e-1P_e$ transition, size tunable in the mid-IR range and with an intensity comparable to the interband exciton. Below, we present similar photoexcitation studies of the PbSe nanocrystals.

After excitation of the PbSe samples with a 1.064 μm pump pulse, a delayed, low power, probe beam shows a strong absorption around mid-gap energy. This absorption displays significant power dependence with decay components as fast as 10−20 ps and slower components similar to the interband bleach dynamics. This behavior is shown in Figure 8. If the energy of the probe beam is varied, as in Figure 9, the delay scans show drastically different kinetics. By taking a series of delay scans at different probe energies, the spectra of the intraband transitions can be constructed. Figure 10 shows the induced IR absorption spectra of several samples of PbSe quantum dots at delay times of 10 and 300 ps. For all samples, the peak absorbance of the photoinduced IR absorption is quite strong, almost equaling the intensity of the first exciton. As the

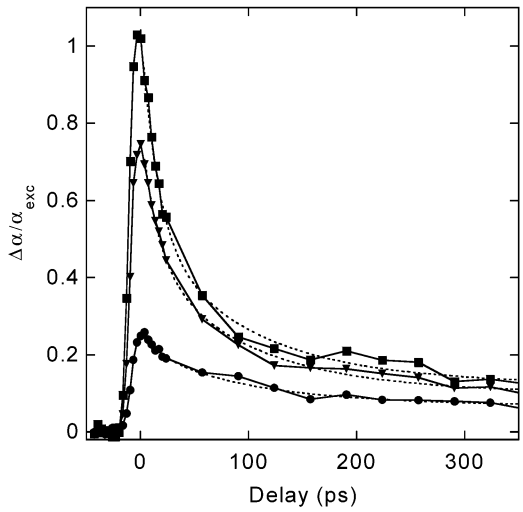

Figure 8. Time-resolved intraband absorption for a 0.817 eV PbSe quantum dot sample in HMN at 7 K and for a range of 1.064 μm pump powers: 7mW (●), 32mW (▼), and 80 mW (■). The curve fits (- -) are triple exponential decays with lifetimes of 15, 85, and 240 ps and an offset.

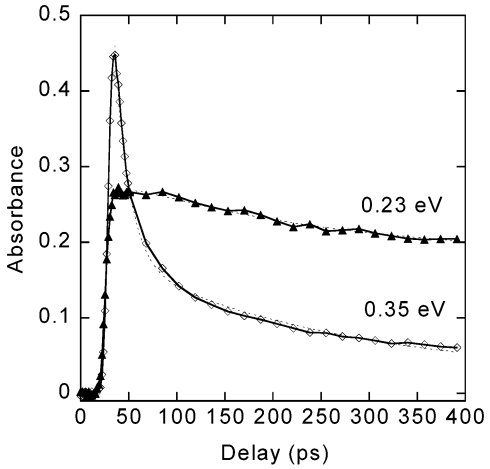

Figure 9. Time-resolved intraband absorption of 0.812 eV PbSe quantum dots at 7K in HMN. The sample was excited by a 1.064 μm pump pulse and probed with photon energies of 0.23 eV (▲) and 0.35 eV (◊). Fits for the data are shown as thin dashed lines. The fits use two exponentials (15 and 240 ps) and a constant offset.

system relaxes, the spectra shift to lower energy and become noticeably narrower and less intense. At early times, the intraband spectra, which are asymmetric with a long tail at high energy, are poorly fit with a single Gaussian. They are best fit by the sum of two Gaussians, one narrow and the other broader and blue shifted. At a delay time of 300 ps only the narrower Gaussian persists, slightly red shifted.

One could attribute these two distinct induced absorptions to the different dynamic behaviors of the hole and the electron. In PbSe, the hole is somewhat lighter than the electron, $m_e = 0.04m_0$ and $m_h = 0.034m_0$ at 4 K. The lighter hole would lead to a higher energy $1S_h-1P_h$ intraband transition, with the fast decay indicating that the hole quickly becomes trapped, while the electron would lead to the long-lived $1S_e-1P_e$ intraband transition that was lower in energy. Fast trapping of the hole is an accepted view for CdSe materials.[26] However, for the PbSe samples, this picture is inconsistent with the high quantum yield, small Stokes shift and the slow interband relaxation. Furthermore, the fast ~10 ps intraband component, which appears at high energy, is not present at all in the interband relaxation data.

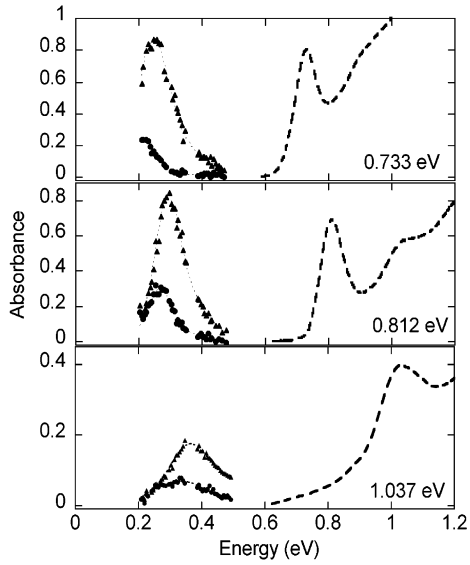

Figure 10. Intraband absorption spectra of three different PbSe quantum dot samples at 7 K in HMN shown beside the room-temperature linear absorption spectra (- -). The intraband spectra are shown at 10 ps (▲) and 300 ps (●) delays of the probe pulse with respect to the 1.064 μm pump pulse. The intraband spectra are fit with two Gaussians at 10 ps and a single Gaussian at 300 ps (fine dotted line).

Instead we propose a model in which the long-lived intraband component is due to transitions from a single electron *and* a single hole occupying the $1S_e$ and $1S_h$ states, respectively. Because the masses of the electron and the hole are quite similar, the two transitions, $1S_e-1P_e$ and $1S_h-1P_h$, are not resolved separately. The fast component is then assigned to transitions that involve electrons and holes in the $1P_e$ and $1P_h$ states making transitions to higher states, such as the 1D or 2S. This scenario explains both the broader width and the fast decay of this component. In the larger two samples studied, the $1S_h-1P_e$, the $1P_h-1S_e$, and the $1P_h-1P_e$ interband transitions are all accessible with the energy of a 1.064 μm photon. Therefore the photoinduced occupation of $1P_{e,h}$ states is taking place. This may explain why the intensity of the induced intraband absorption for the smallest sample is much weaker than the first exciton, whereas the two larger samples exhibit an intensity that is roughly as large as the optical density of the first exciton. At low pump powers the electrons and holes quickly relax to the 1S states. At higher pump powers, the 1S states are filled and the 1P states become occupied. Auger recombination leads to the depletion of the P states first. Since the Auger recombination rate scales as the square of the excitation density, the initial 10−20 ps component is consistent with creation of 4−6 $e^- - h^+$ pairs.

To the assigned $1S_{e,h}-1P_{e,h}$ transition energies, we add the confinement energy of the first exciton and divide by the first exciton confinement energy (this effectively only adds 1 to the ratio of the$1S_{e,h}-1P_{e,h}$ transition energies to the first exciton confinement energy). The results, shown in Figure 3, are compared to the confinement energies of the $1S_h-1P_e$ and $1P_h-1S_e$ second excitons. There is excellent agreement between the second exciton confinement energy and the position of the intraband transition. This supports the assignment of the intraband transition as well as supports the assignment of the second exciton to the $1S_{e,h}-1P_{h,e}$ transitions.

E. Intraband Relaxation. As seen above, the PbSe nanocrystals are a rather simple system with a sparse band structure and no obvious trap states, evidenced by their highly efficient

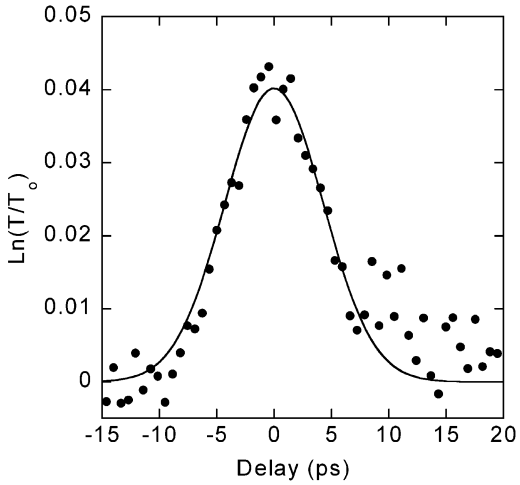

Figure 11. Bleach of $1S_{e,h}-1P_{e,h}$ transition in PbSe quantum dots at 7K in HMN for a sample with a first exciton OD of 0.8 at 0.812 eV. The 1.064 μm excitation of the sample was followed at 350 ps by a pump pulse at 0.269 eV and a resonant probe pulse.

fluorescence. These features make it an ideal system to investigate the phonon bottleneck issue. The phonon bottleneck refers to the expected slow relaxation of excited electronic states in quantum dot systems where the states are separated by more than the energy of two optical phonons.[27] The phonon bottleneck would have significant consequences, such as, for example, allowing intraband radiative emission far into the mid-IR. The LO phonon of PbSe is at 17 meV.[12] Therefore, the sizes studied here are well within the regime for which the phonon bottleneck is expected. In the colloidal quantum dot systems studied so far (CdSe,[28−30] InP,[30] and ZnO[30]) the phonon bottleneck has been elusive, and dominant ps or sub-ps relaxation is usually observed. For single e^-−h^+ pair, the explanation proposed for II−VI and III−V materials has been a fast Auger process between the hole and electron. In the II−VI and III−V's, the valence band is 3-fold nearly degenerate and the mass of the hole is large. This leads to a large density of hole states and it is assumed that hole relaxation proceeds quickly, via phonon emission. The e^-−h^+ Auger process then allows the electron to lose its energy by coupling to the high density of states of the hole.[31] However, it is clear that this model does not apply to the PbSe nanocrystals since both the hole and the electron have a sparse density of state.

An earlier interband study of PbSe in glasses showed fast relaxation between different exciton levels and the absence of the phonon bottleneck.[6] However, these glass samples also showed fast nonradiative relaxation indicating the role of trapping processes.

Intraband bleaching studies on the highly fluorescent colloids were therefore undertaken. The laser setup was modified accordingly. A 1.064 μm pulse creates an e^-−h^+ pair. At some delay (typically 350 ps, to ensure that only one electron and one hole in the $1S_e-1S_h$ are present in the quantum dot), a pump pulse in the mid-infrared, tuned to the intraband transition, promotes electron or hole, or both to their 1P states. Then a tunable probe beam, centered at the pump frequency, follows the transient hole burning in the intraband absorption. Figure 11 shows the bleach in the intraband absorbance at 7 K as a function of delay time for the PbSe sample with a room temperature first exciton at 0.812 eV. The magnitude of the bleach signal is small, 4% and the lifetime is shorter than our laser can resolve and therefore is <4 ps. Similar results were observed for larger dots and no bleach could be obtained for smaller dots. Thus, there appears to be *no* phonon bottleneck in PbSe colloidal quantum dots. This is not understood and there is a need for a novel mechanism to explain these results. It may be that very strong acoustic coupling reduces the lifetime of the excited state or that surface effects play an unexpected role in the relaxation process.

IV. Conclusion

We presented a study of the interband and intraband transitions of oleic acid-capped PbSe colloidal quantum dots. These nanocrystals exhibit a size-dependent first exciton, which tunes from 0.5 to 1 eV (2.5 μm to 1.25 μm). The well-defined linear absorption interband spectra not only reveal the monodisperse nature of the colloids, but also reflect the simpler band structure of PbSe, as compared to II−VI and III−V semiconductors. We have observed the $1S_{e,h}-1P_{e,h}$ tuning between 0.2 and 0.33 eV as a function of size. At high pump intensities, we have also observed a broader and short-lived resonance that we assign to $1P_{e,h}-1D_{e,h}$ transitions. The assignment of the interband excitonic structure is based on the straightforward effective mass approximation. Despite the simplicity of this approach, the assignments, when coupled with the intraband spectra, do create a consistent picture. Two remaining questions are why the second exciton is optically allowed and why the expected 4-fold degeneracy of the quantum states[9] is not apparent in the bleach data.

The PbSe dots are efficient near-infrared fluorophores with small Stokes shift and lifetimes close to a microsecond, at least 3 orders of magnitude shorter than rare earth infrared fluorophores. Interband bleach experiments reveal that the first exciton decays with a long lifetime consistent with radiative relaxation, except at higher excitation energies where the relaxation is dominated by Auger recombination.

Finally we directly measured the lifetime of the $1P_{e,h}$ state in PbSe quantum dots to be less than 4 ps. In these high-quality quantum dots, with low optical phonon frequency, no obvious trap states, and a sparse density of quantum-confined states, such a fast intraband relaxation cannot be simply accounted for by the current models. This fact reflects a basic misunderstanding of carrier dynamic in colloid quantum dots and remains to be explained.

The PbSe nanocrystal colloids represent a new opportunity for nanoscale optical materials. The synthetic procedures are simpler than for II−VI materials, while the quality is at least equivalent and the spectral structure is simpler. Of immediate interest is the infrared ranges that PbSe quantum dots cover. PbSe, and IV−VI materials in general, have material properties that are rather unusual, with very large optical and d.c. dielectric constants. Following the growing literature on quantum well structures based on IV−VI materials, natural extensions of the synthetic work are the control of the shape, the formation of core−shell structures and the doping of donor/acceptor or magnetic impurities.

Acknowledgment. We acknowledge helpful conversations with Dr. Margaret A. Hines. Lattice resolution TEM images were taken by Prof. J. -G. Zheng at the EPIC center at Northwestern University. This work was funded by U.S. National Science Foundation (NSF) under Grant DMR-0108101. The authors made use of the MRSEC Shared Facilities supported by NSF under Grant DMR-9400379.

References and Notes

(1) Nirmal M.; Brus L. E. *Acc. Chem. Res.* **1999**, *32*, 407.
(2) Efros A. L.; Rosen M. *Annu. Rev. Mater. Sci.* **2000**, *30*, 475.

(3) Lipovskii, A.; Kolobkova, E.; Petrikov, V.; et al. *Appl. Phys. Lett.* **1997**, *71*, 3406.
(4) Guerreiro, P. T.; Ten, S.; Borelli, N. F.; et al. *Appl. Phys. Lett.* **1997**, *71*, 1595.
(5) Olkhovets, A.; Hsu, R.-C.; Lipovskii, A.; Wise, F. W. *Phys. Rev. Lett.* **1998**, *81*, 3539.
(6) Wundke, K.; Potting, S.; Auxier, J.; et al. *Appl. Phys. Lett.* **2000**, *76*, 10.
(7) Wunkde, K.; Auxier, J.; et al. *Appl. Phys. Lett.* **1999**, *75*, 3060.
(8) Wise, F. W. *Acc. Chem. Res.* **2000**, *33*, 773.
(9) Kang, I.; Wise, F. W. *J. Opt. Soc Am. B.* **1997**, *14*, 1632 1997.
(10) Nenadevic, M. T.; Comor, M. I.; Vasic, V.; Micic, O. I. *J. Phys. Chem.* **1990**, *94*, 6390.
(11) Murray, C. B.; Sun, S. H.; Gaschler, W.; et al. IBM. *J. Res. Dev.* **2001**, *45*, 47.
(12) Landolt-Bornstein. *Semiconductors: Physics of Nontetrahedrally Bonded Binary Compounds II*; Springer-Verlag: Berlin, 1983; Vol. III/17f.
(13) Andreev, A. D.; Lipowskii, A. *Phys. Rev. B.* **1999**, *59*, 15402.
(14) Shim, M.; Guyot-Sionnest, P. *J. Chem. Phys.* **1999**, *111*, 6955.
(15) Kuno, M.; Lee, J. K.; Dabbousi, B. O.; Mikulec, F. V.; Bawendi, M. G. *J. Chem. Phys.* **1997**, *106*, 9869.
(16) Seilmeir, A.; Kopainsky, B.; Kaiser, W. *Appl. Phys.* **1980**, *22*, 355.
(17) Kopainsky, B.; Qiu, P.; Kaiser, W.; Sens, B.; Drexhage, K. H. *Appl. Phys. B.* **1982**, *29*, 15.
(18) Cao, Y. W.; Banin, U. *J. Am. Chem. Soc.* **2000**, *122*, 9692.
(19) Harrison, M. T.; Kershaw, S. V.; Rogach, A. L.; Kornowski, A.; Eychmuller, A.; Weller, H. *Adv. Mater.* **2000**, *12*, 123.
(20) Norris D. J.; Bawendi, M. G. *Phys. Rev. B* **1996**, *53*, 16338.
(21) Efros, Al. L.; Rodina, A. V. *Phys. Rev. B* **1993**, *47*, 10005.
(22) Landolt-Bornstein. New Series III/141B; Springer: Berlin, 1999.
(23) Klann, R.; Hofer, T.; Buhleier, R.; Elsaesser, T.; Tomm, J. W. *J. Appl. Phys.* **1995**, *77*, 277.
(24) Gmachl, C.; Capasso, F.; Sivco, D. L.; Cho, A. Y. *Rep. Prog. Phys.* **2001**, *64*, 1533.
(25) Guyot-Sionnest, P.; Shim, M.; Wang, C. In *Chemically Synthesized Quantum Dots*; Klimov, V. I., Ed.; Marcel Dekker: New York. To be published.
(26) Klimov, V. I. *J. Phys. Chem. B.* **2000**, *104*, 6112.
(27) Bockelmann, U.; Bastard, G. *Phys. Rev. B.* **1990**, *42*, 8947.
(28) Klimov, V. I.; McBranch, D. W. *Phys. Rev. Lett.* **1998**, *80*, 4028.
(29) Guyot-Sionnest, P.; Shim, M.; Matranga, C.; Hines, M. A. *Phys. Rev. B.* **1999**, *60*, 2181.
(30) Shim, M.; Guyot-Sionnest, P. *Phys. Rev. B.* **2001**, *64*, 245342.
(31) Efros, A. L.; Kaharchenko, V. A.; Rosen, M. *Solid State Commun.* **1995**, *93*, 281.